

# The $A_4$ glass transition singularity

S. Flach<sup>1,\*</sup>, W. Götze<sup>2</sup>, and L. Sjögren<sup>3</sup>

<sup>1</sup> Institut für Theoretische Physik, Technische Universität Dresden, Mommsenstrasse 13, O-8027 Dresden, Federal Republic of Germany

<sup>2</sup> Physik-Department, Technische Universität München, W-8046 Garching and Max-Planck-Institut für Physik und Astrophysik, W-8000 München, Federal Republic of Germany

<sup>3</sup> Institute of Theoretical Physics, Chalmers University of Technology, S-41296 Göteborg, Sweden

Received December 16, 1991

Formulae for the  $\beta$ -relaxation process as obtained within the mode coupling theory for the dynamics of supercooled liquids are derived for states near an  $A_4$  glass transition singularity. A discussion of the expected anomalies of susceptibility spectra is presented. In particular the parameter regions for  $(1/f)$ -noise, for spectra exhibiting two minima and regions of linear variations in  $\ln(1/f)$  are identified. The results are used to interpret quantitatively dielectric data for the following polymeric systems: polychlorotrifluoroethylene (PCTFE), polyhexamethylene sebacamide (nylon 610), polyoxymethylene (delrin) and polyparaethylene oxybenzoate (PEOB).

## 1. Introduction

In recent years the mode coupling theory (MCT) of supercooled liquid dynamics has been developed and applied to predict and to analyse spectra of glass forming systems. The essence of the theory are bifurcation singularities of the cuspid type  $A_l$  ( $l=2, 3, 4, \dots$ ) [1], [2]. These singularities appear in equations of motion which were derived by certain factorization approximations carried out for the dynamics of simple liquids. Thereby a new small parameter was discovered, viz the separation from the mentioned singularities. This small parameter allows for asymptotic solutions of the complicated equations of motion. These solutions are proposed as qualitative or even quantitative explanations of the relaxation properties in complex glassy systems. A review, reflecting the state of the art two years ago, can be found in [3]. The simplest singularity  $A_2$ , the Whitney fold, describes generically the ideal transition from ergodic dynamics for a liquid to non-ergodic dynamics for an ideal glass state. The  $A_3$  singularity, the Whitney cusp, appears as the endpoint singularity of  $A_2$  transition hypersurfaces. In this paper the dynamics near an  $A_4$  singularity shall be dis-

cussed and some dielectric loss data for polymers will be analyzed within the  $A_4$  scenario.

The MCT deals with a set of  $M$  correlators  $\Phi_q(t)$  as functions of the label  $q=1, 2, \dots, M$  and time  $t$  or with their Laplace transforms  $\Phi_q(z) = LT[\Phi_q(t)](z)$  as function of complex frequency  $z = \omega + i0$ . The initial conditions are given by  $\Phi_q(t=0) = 1$ ,  $\partial_t \Phi_q(t=0) = 0$ . The functions have to be calculated as solutions of the following three equations.

$$\partial_t^2 \Phi_q(t) + \Omega_q^2 \Phi_q(t) + \nu_q \partial_t \Phi_q(t) + \Omega_q^2 \int_0^\infty dt' m_q(t-t') \partial_{t'} \Phi_q(t') = 0 \quad (1.1)$$

is a typical Zwanzig-Mori equation of motion. The frequencies  $\Omega_q > 0$ ,  $\nu_q > 0$  describe restoring forces for oscillations and a stochastic friction respectively. They specify the microscopic transient motion or the microscopic excitation band of the spectra. All dynamic effects due to degrees of freedom, not accounted for by the  $M$  correlators, are hidden in the generalized friction kernel  $m_q(t)$ , which can be considered as a fluctuating force correlation function [4]. The kernel is given as a mode coupling functional in terms of the correlators

$$m_q(t) = F_q(\mathbf{V}, \Phi_q(t)). \quad (1.2)$$

Generalizing the original derivation [5], [6] somewhat, the functional is written down as an arbitrary polynomial:

$$F_q(\mathbf{V}, f_k) = \sum_k V_{q,k} f_k + \frac{1}{2} \sum_{k,j} V_{q,k,j} f_k f_j + \dots \quad (1.3)$$

The vertices  $V_{q,k} \geq 0$ ,  $V_{q,k,j} \geq 0, \dots$ , are the coupling constants of the theory. They are combined to the mathematical control parameter vector  $\mathbf{V}$  in some  $N$ -dimensional control parameter space  $\mathcal{X}$ . In applications, one expresses  $\mathbf{V}$  in terms of physical control parameters like temperature  $T$ , density  $n$  or crystallinity  $x$ . So, in the simplest case, the system moves on a path  $C$ ,  $T \rightarrow \mathbf{V}(T)$ , through  $\mathcal{X}$ . The specified problem has a unique solution

\* Research Fellow of the Alexander-von-Humboldt-Foundation

which depends smoothly on  $\mathbf{V}$  for all finite time intervals; the correlators have the proper analytic properties [7]. The mentioned equations formulate only the simplest version of the MCT, implying an ideal liquid glass transition, to which we restrict our attention in this paper.

The long time limit  $f_q(\mathbf{V}) = \Phi_q(t \rightarrow \infty)$  is a solution of the set of  $M$  coupled algebraic equations [5]:

$$\frac{f_q}{1 - f_q} = F_q(\mathbf{V}, f_k). \quad (1.4)$$

In general there are several solutions obeying  $0 \leq f_q^{(\alpha)} \leq 1$ ,  $\alpha = 1, 2, \dots$ . The long time limit of  $\Phi_q(t)$  is the maximum [3]:

$$f_q(\mathbf{V}) = \max(f_q^{(\alpha)}). \quad (1.5)$$

The space  $\mathcal{N}$  is the union of the open set  $\mathcal{D}_{\mathcal{L}}$ , containing a neighbourhood of the weak coupling limit  $\mathbf{V} \rightarrow 0$ , the open set  $\mathcal{D}_{\mathcal{H}}$ , containing a neighbourhood of the strong coupling limit  $\mathbf{V} \rightarrow \infty$ , and the closed hypersurface  $\mathcal{D}_{\mathcal{S}}$ , separating  $\mathcal{D}_{\mathcal{L}}$  and  $\mathcal{D}_{\mathcal{H}}$ .  $\mathbf{V} \in \mathcal{D}_{\mathcal{L}}$  are called liquid states, since they refer to ergodic motion  $f_q(V) = 0$ . The states  $\mathbf{V} \in \mathcal{D}_{\mathcal{H}}$  have a non-trivial long time limit  $f_q(V) > 0$ , which depends smoothly on  $\mathbf{V}$ . These are ideal glass states [8]. The Edwards-Anderson parameter  $f_q(V)$  or non-ergodicity parameter, or form factor specifies the stability of the glass states. For  $\mathbf{V} = \mathbf{V}_c \in \mathcal{D}_{\mathcal{S}}$  the function  $f_q(\mathbf{V})$  exhibits singularities, called glass transition singularities [9]. These are bifurcation singularities of (1.4) obeying (1.5).

The special properties of functional  $F_q$  ensure, that the critical points  $\mathbf{V}_c$  are caused by a non-degenerate eigenvalue of the Jacobian matrix of (1.4) to vanish [10], [11], and therefore the singularities are cuspsoids  $A_l$  ( $l \geq 2$ ) [1], [2]. One can prove the factorization theorem [10], [11]

$$\Phi_q(t) = f_q^c + h_q G(t) \quad (1.6)$$

for  $\mathbf{V}$  near  $\mathbf{V}_c$  and  $\Phi_q(t)$  near  $f_q^c = f_q(V_c)$ . The critical amplitude  $h_q$  can be evaluated from the relevant eigenvector of the mentioned Jacobi matrix. The time or frequency window, where (1.6) applies, is called  $\beta$ -relaxation region. It excludes the short time transient motion, i.e.  $t_0 \ll t$ , but also the long time  $\alpha$ -dynamics, i.e.  $t \ll \tau_\alpha$ . For a precise definition, see Eqs. (2.15) and (2.20) below. If one considers correlations of variables  $X, Y$ , having some overlap with density fluctuation products, one may generalize (1.6) to

$$\Phi_{XY}(t) = f_{XY}^c + h_{XY} G(t). \quad (1.7)$$

There enter different time-independent quantities  $f_{XY}^c, h_{XY}$  but the time variation is given by the same  $\beta$ -correlator  $G(t)$  as in (1.6). This is a kind of universality of the  $\beta$ -dynamics. Examples, where (1.7) is predicted to be valid, are auto correlation functions,  $X = Y$ , for longitudinal elastic modulus, shear stress fluctuations, dielectric functions, dielectric moduli, coherent and incoherent neutron scattering cross sections.

In the simplest case of an  $A_2$  singularity the correlator  $G$  obeys a one parameter scaling law [10], [11]. The theoretical results have in this case been compared with dielectric loss spectra for amorphous polyethylene terephthalate (PET) [12] and polyethylene oxybenzoate (PEOB) [13], with photon correlation decay curves for hard sphere colloids [14] and with molecular dynamics results for tagged particle motion in a binary mixture [15]. A rather extensive study of  $\beta$ -relaxation at an  $A_2$  fold for a conventional glass former,  $\text{CaKNO}_3$ , has been carried out recently for light scattering spectra by Cummins and collaborators [16]. In this case spectra were studied for a four decade frequency window and the theoretical predictions were found to hold for the rather large temperature interval extending from 20 °C to 190 °C. The ideal glass transition temperature  $T_c$ , defined by  $\mathbf{V}(T_c) = \mathbf{V}_c$ , was found to be  $(105 \pm 5)$  °C, i.e. it is located about 45 °C above to calorimetric glass transition temperature  $T_g$ .

The correlator  $G(t)$  for an  $A_l$  singularity with  $l \geq 3$  can be expressed in leading order in terms of hyperelliptic functions [17]. This simplifies the theoretical discussion to the evaluation of an integral. It was shown recently [13], that dielectric functions of polychlorotri-fluoroethylene (PCTFE) follow an  $A_3 - \beta$ -relaxation pattern. The  $A_l$  scenario contains  $A_k$ -patterns as special limits for  $k < l$ . As a result one obtains  $A_k$  relaxation patterns, which exhibit distortions due to  $A_l$  relaxation precursors. This was demonstrated to be the case for PET-IV and PEOB-IV [13]. These are polymers mentioned above containing a considerable percentage of crystallinity. In these examples the  $A_2$ -loss spectra were distorted by the presence of an  $A_3$  glass transition singularity.

The present paper extends the preceding work by a discussion of the  $A_4$ - $\beta$ -relaxation correlator  $G(t)$ . It is motivated by two questions. What are the typical distortions of  $A_3$ -spectra due to the presence of an  $A_4$ -singularity? What are the characteristic  $A_4$ - $\beta$ -relaxation features, which cannot be described by  $A_2$  or  $A_3$  relaxation patterns?

## 2. Basic formulae

### 2.1. The separation parameters

Let us recall the theory of the solution of (1.4) in the neighbourhood of an  $A_4$  singularity  $\mathbf{V}_c$ ,  $f_q(\mathbf{V}_c) = f_q^c$ . For  $\mathbf{V} \rightarrow \mathbf{V}_c$  one gets in leading order

$$f_q = f_q^c + h_q \cdot \rho^2 \cdot \delta f. \quad (2.1)$$

Here  $\rho^2$  is a constant factor [17], which could be absorbed in  $h_q$ . The space of perturbations is 3-dimensional [1], [2]. In our terminology this result of singularity theory shall be formulated as follows. There are three smooth functions of the mathematical control parameters which are denoted as  $g_k(\mathbf{V})$  for  $k = 2, 3, 4$ ; they vanish at the singularity,  $g_k(\mathbf{V}_c) = 0$ . The leading contribution  $\delta f$  depends on the three relevant control parameters  $g_k(\mathbf{V})$  as a solution of the algebraic equation:

$$S(\delta f) = 0, \quad (2.2)$$

$$S(u) = u^4 - g_2 \cdot u^2 - g_3 \cdot u - g_4. \quad (2.3)$$

These  $g_k$  are referred to as the separation parameters. It is the essential complication of an  $A_4$  singularity as opposed to an  $A_2$  or  $A_3$  singularity, that three parameters  $g_k$  rather than one or two in the simpler cases, are needed in order to specify the sensitive part of  $f_q - f_q^c$ . The results (2.2), (2.3) are derived from a more general solution near singularities  $A_k$ ,  $k \geq 3$  [13], where  $S(u)$  has to be replaced by a polynomial of degree  $k$   $S_k(u; g_2, \dots, g_k)$ .

Three independent physical control parameters  $X_i$ ,  $i = 1, 2, 3$ , are needed in order to scan the relevant part of the  $A_4$  singularity neighbourhood:  $\mathbf{V} = \mathbf{V}(X_1, X_2, X_3)$ . Let  $X_i^c$  specify the singularity  $\mathbf{V}_c = \mathbf{V}(X_1^c, X_2^c, X_3^c)$ . Then the separation parameters can be represented in leading order for small  $(X_i - X_i^c)$  as:

$$g_k = \sum_{i=1}^3 C_{ki} \cdot (X_i - X_i^c), \quad k = 2, 3, 4. \quad (2.4)$$

The invertable matrix  $C_{ki}$  connects the physical control parameters with the relevant mathematical ones. For every given model of the MCT, specified by (1.1)–(1.3), one can calculate the  $g_k$  or the matrix  $C$  straight forwardly.

A scaling line  $L^0$  through the parameter point  $g_k^0$  shall be defined by

$$g_k(s) = g_k^0 \cdot s^{k^c}, \quad k = 2, 3, 4. \quad (2.5)$$

Variable  $s \geq 0$  is the line parameter. Moving along  $L^0$  the solution of (2.2), (2.3) varies linearly with  $s$ :

$$\delta f = \delta f^0 \cdot s. \quad (2.6)$$

Inverting (2.4), (2.5) one can represent  $L^0$  as a map of  $X_i = X_i(s)$ ,  $X_i(s=0) = X_i^c$ . Thus a scaling line is obtained as map of a path  $L: s \rightarrow \mathbf{V}(s)$  in the general control parameter space  $\mathcal{X}$ . The concept of a leading order result can now be given as the formula

$$\lim_{s \rightarrow 0} \frac{f_q(\mathbf{V}(s)) - f_q^c}{h_q \cdot \rho^2 \cdot \delta f} = 1. \quad (2.7)$$

Corrections to the formulae (2.1), (2.6) vanish faster than  $s$  if one approaches  $V_c$  on the scaling line  $L$  by the limit procedure  $s \rightarrow 0$ .

## 2.2. The three parameter scaling law

The preceding formulae (2.1), (2.6), (2.7) can be generalized for the  $\beta$ -correlator in (1.6). It can be written as function  $p$  of the logarithm of the time:

$$G(t) = \rho^2 \cdot p(y), \quad (2.8)$$

$$y = \ln \left( \frac{t}{t_1} \right). \quad (2.9)$$

Here  $t_1$  is a scale for the short time transient motion. It varies smoothly with  $\mathbf{V}$ ; in leading order it can be replaced by its value at the singularity. Function  $p$  is a solution of

a differential equation, governed by the separation parameters:

$$p_{,y}^2 = S(p), \quad (2.10)$$

where  $p_{,y} = dp/dy$ . It has to be solved with the initial condition

$$p(y \rightarrow 0) = \frac{1}{y}. \quad (2.11)$$

Function  $p$  decreases monotonically with increasing  $y$ . Either it arrests at the value  $\delta f$  or it keeps on decreasing till the regime of  $\beta$ -relaxation terminates. In the former case  $p$  remains constant for large times as expected for an ideal glass state. The described function is a hyper-elliptic one,

$$p(y) = p(y; g_2, g_3, g_4), \quad (2.12)$$

which is the inverse of the elliptic integral:

$$y = \int_p^{\infty} \frac{ds}{\sqrt{S(s)}}. \quad (2.13)$$

Function  $p$  exhibits the homogeneity:

$$p \left( \frac{y^0}{s}; g_2^0 \cdot s^2, g_3^0 \cdot s^3, g_4^0 \cdot s^4 \right) = s \cdot p(y^0; g_2^0, g_3^0, g_4^0). \quad (2.14)$$

This is a three parameter scaling law: approaching  $\mathbf{V}$  on a scaling line  $L$ , the correlator  $G$  decreases linearly with the parameter  $s$ , provided the time scales to infinity according to  $y = y^0/s$  or  $t = t_1 \cdot (t_0/t_1)^{1/s}$ . This result allows for the precise definition of the formulated leading order  $\beta$ -relaxation formulae:

$$\lim_{s \rightarrow 0} \frac{\Phi_q(t) - f_q^c}{h_q \cdot \rho^2 \cdot p \left( \frac{1}{s} \cdot \ln \left( \frac{t}{t_1} \right); g_2(s), g_3(s), g_4(s) \right)} = 1. \quad (2.15)$$

Details of the proofs can be found in [17].

Equations (2.8), (2.9), (2.10) comprise the essence of the mode coupling equations (1.1)–(1.3). The interplay of non-linearities with retardation effects leads to bifurcations for the motion. The latter are connected with a change of the time in the original equations of motion to  $\ln(t)$  in the equations ruling the slow dynamics near a bifurcation point. This in turn explains the most important feature of glassy relaxation, i.e. the stretching of the dynamics over huge time windows.

## 2.3. The low frequency susceptibilities

An essential mathematical tool in the proof of (2.15) is a proper generalization of formulae for Laplace transforms of slowly varying functions [17]. Let us note the leading order result for the  $\beta$ -relaxation result (1.6), (1.7). It shall be specialized for the dielectric function  $\varepsilon(\omega) = \varepsilon'(\omega) + i\varepsilon''(\omega)$ . The two constants in (1.7) will be denoted by  $f_c$  and  $\varepsilon_c$  respectively. One gets

$$\varepsilon'(\omega) = f_c - \varepsilon_c \cdot p(u), \quad (2.16)$$

$$\varepsilon''(\omega) = -\frac{\pi}{2} \cdot \varepsilon_c \cdot p_{,u}(u). \quad (2.17)$$

Here  $u$  is the logarithm of the frequency

$$u = \ln \left( \frac{1}{\omega t_1} \right), \quad (2.18)$$

and the derivative  $p_{,u}(u)$  of  $p(u)$  follows from (2.12), (2.13) to

$$p_{,u}(u) = -\sqrt{S(p(u))}. \quad (2.19)$$

Formulae (2.16), (2.17) follow for  $u \rightarrow 0$  from (2.8), (2.9) if  $p(y)$  is slowly varying [18]. The quoted result is valid more generally. It formulates the asymptotic result for the variation of  $\varepsilon(\omega)$  upon approaching  $\mathbf{V}$  on the scaling line  $L$ :

$$\lim_{s \rightarrow 0} \frac{\varepsilon(\omega) - f_c}{(p + i \frac{\pi}{2} \cdot p_{,u}) \cdot \frac{u_0}{s}} = -\varepsilon_c. \quad (2.20)$$

### 3. Critical dynamics

#### 3.1. Glass transition singularities

Bifurcation points of type  $A_l$ ,  $l=2, 3, 4$ , for the solution  $\delta f$  of (2.2), (2.3) are given by those parameter triples  $(g_2, g_3, g_4)$ , where polynomial  $S(u)$  has a zero  $\xi$  of multiplicity  $l$ . The condition  $S(\xi) = 0$ ,  $S_{,\xi}(\xi) = 0$  implies one relation among the separation parameters, and this specifies the bifurcation surface  $\mathcal{H}$ . The latter can be described by two Gaussian surface parameters. Let us choose them as the zero  $\xi$  and the leading Taylor coefficient  $\eta$  at the zero:  $S(u) = (u - \xi)^2 \cdot \eta + O((u - \xi)^3)$ . If one observes, that the sum of the zeroes of  $S$  vanishes, one can write for the points on  $\mathcal{H}$ :

$$\mathcal{H}: S(u) = (u - \xi)^2 \cdot [(u - \xi)^2 + 4\xi(u - \xi) + \eta]. \quad (3.1)$$

Comparison with (2.3) yields the parameter representation of  $\mathcal{H}$ :

$$\mathcal{H}: \begin{aligned} g_2 &= 6\xi^2 - \eta, & g_3 &= 2\xi(\eta - 4\xi^2), \\ g_4 &= \xi^2(3\xi^2 - \eta). \end{aligned} \quad (3.2)$$

Obviously,  $\mathcal{H}$  is symmetric under substitution  $\xi \rightarrow -\xi$  or  $g_3 \rightarrow -g_3$ . The root  $\xi$  has multiplicity 2 if and only if  $\eta \neq 0$ . Thus the inner points of  $\mathcal{H}$ , the  $A_2$  bifurcations, are given by

$$A_2: \xi \in (-\infty, \infty), \eta \neq 0. \quad (3.3)$$

Two cusp lines are obtained as the endpoints

$$A_3: \eta = 0 \text{ and } \xi \in (-\infty, 0) \text{ or } \xi \in (0, \infty), \quad (3.4)$$

while the  $A_4$ -singularity is described by

$$A_4: \xi = 0, \eta = 0. \quad (3.5)$$

Scaling lines on  $\mathcal{H}$  are given by the parameter representation

$$\xi = s \cdot \xi_0, \eta = s^2 \cdot \eta_0, 0 < s < \infty. \quad (3.6)$$

The two solutions of  $S(u) = 0$ , which occur in addition to  $\xi$ , are given by  $u_{\pm} = -\xi \pm \sqrt{4\xi^2 - \eta}$ . The points of  $\mathcal{H}$  are glass transition singularities if and only if (1.5) is valid. This  $\mathcal{D}_{\mathcal{H}}$  is characterized by such points  $(\xi, \eta)$ , where  $u_{\pm}$  are not real or where  $\xi \geq u_{\pm}$ :

$$4\xi^2 < \eta \text{ or } 0 < \xi \text{ and } 0 \leq \eta. \quad (3.7)$$

Because of the scaling properties,  $\mathcal{H}$  or  $\mathcal{D}_{\mathcal{H}}$  are fully characterized by the three cuts with the planes  $g_2 = 1, 0, -1$ . The cuts are shown as full lines in Figs. 1, 2, 3. They can be given easily in parameter representation. The arrows indicate the direction of increasing  $\xi$ . From (3.2) one finds for the first cut

$$g_2 = 1: \eta = 6\xi^2 - 1. \quad (3.8)$$

The restriction (3.7) is equivalent to

$$1 < 2\xi^2 \text{ or } 0 < \xi \text{ and } 1 < 6\xi^2. \quad (3.9)$$

The part of  $\mathcal{H}$ , which does not belong to  $\mathcal{D}_{\mathcal{H}}$  is included in Fig. 1 in dotted, so that the reader can recognize the familiar swallow tail structure [1], [2]. The intersection with the cusp lines, shown as open circles, have coordinates  $\xi = -1/\sqrt{6}$  (belonging to  $\mathcal{H}$  but not to  $\mathcal{D}_{\mathcal{H}}$ ) and  $\xi = 1/\sqrt{6}$  (belonging to  $\mathcal{D}_{\mathcal{H}}$ ). The line  $1/\sqrt{6} < \xi < \infty$  stops the line for negative  $\xi$  at the crossing singularity  $\xi = -1/\sqrt{2}, \eta = 2$ . At  $g_2 = 1, g_3 = 0, g_4 = -1/4$  there is a corner due to self intersections of  $\mathcal{H}$ . The second cut

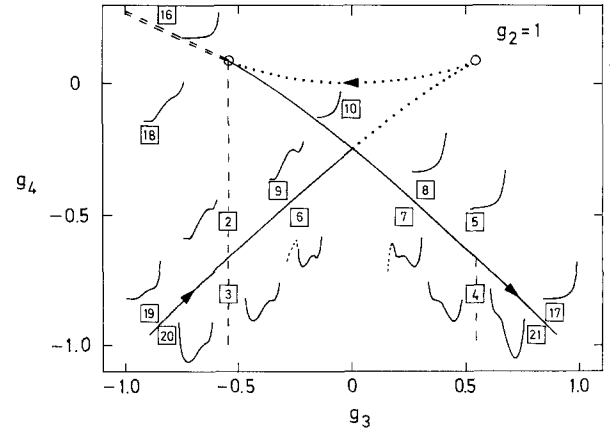


**Fig. 1.** Cut of the bifurcation hypersurface  $\mathcal{H}$  with the plane  $g_2 = 1$  (solid and dotted lines). Open circles:  $A_3$  singularities; dashed lines:  $1/f$  noise hypersurface  $\mathcal{H}_f$ ; double dashed line: hypersurface  $\mathcal{H}_{\log}$  (see text); inserted curves:  $\varepsilon''(\log(\omega))$ , their parameter sets are the midpoints of the corresponding numbered squares (see text)

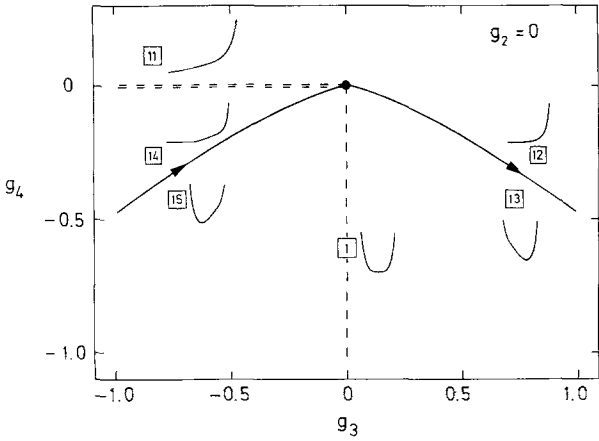


Fig. 2. Same as in Fig. 1 but for the cut with the plane  $g_2 = 0$ . Filled circle:  $A_4$  singularity

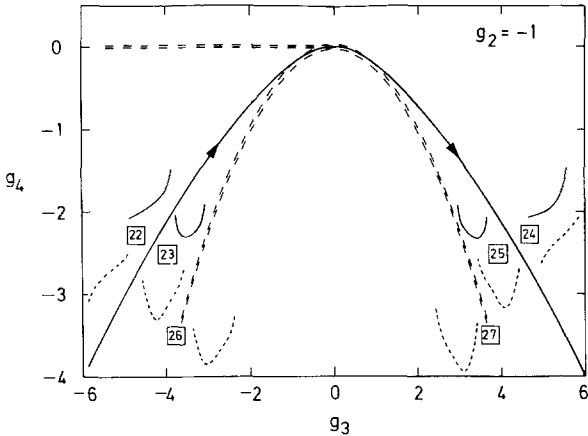


Fig. 3. Cut of the bifurcation hypersurface  $\mathcal{H}$  with the plane  $g_2 = -1$  (solid line). Double dashed parabola: hypersurface  $\mathcal{H}'_{\log}$  (see text); inserted solid curves: same as in Figs. 1, 2; inserted dashed curves: corresponding  $\log e''$  ( $\log(\omega)$ ) dependence

combines two scaling lines and the  $A_4$  singularity, shown by a full circle in Fig. 2:

$$g_2 = 0: g_3 = 4 \xi^3, \quad g_4 = -3 \xi^4. \quad (3.10)$$

The third cut, shown in Fig. 3, is a smooth curve

$$g_2 = -1: \eta = 6 \xi^2 - 1. \quad (3.11)$$

Notice, that all three curves approach the limit curve (3.10) if  $6 \xi^2 \gg 1$ .

### 3.2. Critical correlators

Substitution of (3.1) into (2.13) yields the critical correlators, i.e. the correlation functions at the glass transition singularities  $\mathbf{V}_c \in \mathcal{D}_{\mathcal{Z}}$ :

$$p(y) - \xi = 2\eta \cdot e^{y\sqrt{\eta}} \frac{\sqrt{\eta} + 2\xi}{[e^{y\sqrt{\eta}}(\sqrt{\eta} + 2\xi) - 2\xi]^2 - \eta}. \quad (3.12)$$

For  $y \rightarrow 0$  the r.h.s. of this result exhibits the critical asymptote (2.11). Formula (3.12) stops to be valid at such large  $y_0$ , where  $p(y_0) = \xi$ . In this case  $p(y) \equiv \xi$  for  $y \geq y_0$ .

Near the  $A_3$ -lines one can treat  $y\sqrt{\eta}$  as a small parameter. One gets in leading order the simplification

$$p(y) = \xi + \frac{1}{y + \xi y^2}, \quad y\sqrt{\eta} \ll 1. \quad (3.13)$$

For  $y|\xi| \ll 1$  the correlator approaches the  $A_4$ -critical decay (2.11) while the opposite limit  $y|\xi| \gg 1$  reproduces the  $A_3$ -critical law  $1/(\xi y^2)$  [17]. Formula (3.13) is an example for the modification of an  $A_3$ -result due to the presence of an  $A_4$  singularity. The latter modifies the expected  $A_3$ -result for small  $y$ , i.e. there is a time region between the microscopic time  $t_1$  and long times where the  $A_4$  critical decay holds before the  $A_3$  critical decay takes over.

Off the  $A_3$ -lines one can use  $\exp(-y\sqrt{\eta}) = (t_1/t)^a$  as a small parameter for the long time decay. With the notation

$$a = \sqrt{\eta}, \quad A = \frac{2\eta}{\sqrt{\eta} + 2\xi}, \quad (3.14)$$

one rederives the power law decay of the  $A_2$ -glass transition singularity:

$$p(y) = \xi + A \cdot \left(\frac{t_1}{t}\right)^a, \quad y\sqrt{\eta} \gg 1. \quad (3.15)$$

The presence of an  $A_4$  singularity is reflected by the singular  $\xi - \eta$ -dependence of  $A$ . Approaching  $A_4$  is signaled by the exponent  $a$  to vanish. The formula (2.17) gives the correct spectrum (3.15) only in leading order for  $a \rightarrow 0$ .

## 4. The $\beta$ -susceptibility spectra

A sensitive representation of the various relaxation features is given by the conventional semilogarithmic plots of the susceptibility spectra. From (2.13), (2.17), (2.19) we get

$$\varepsilon''(\omega) \propto \sqrt{S(p(u))}, \quad u = -\ln(\omega t_1). \quad (4.1)$$

Function  $p$  decreases monotonically with increasing  $u$ . Thus the qualitative behaviour of the  $\varepsilon''$  versus  $\log(\omega)$  curves follows from those of the  $S(p)$  versus  $p$  diagrams. We are concerned only with that interval  $p \in (\xi, \infty)$ , where  $S \geq 0$ .

### 4.1. The $1/f$ -noise hypersurfaces

Parameter regions of particular interest are those of  $1/f$ -noise behaviour. Exact  $1/f$ -noise is present, if  $\varepsilon''$  is frequency independent. A well developed approximate  $1/f$ -noise region is observed if  $S(p)$  exhibits a horizontal inflection point  $\kappa$ . Observing, that the sum of the zeroes of  $S$  vanishes, horizontal inflection points of  $S$  versus  $u$

curves are specified by two parameters, which we choose as  $\kappa$  and  $\zeta = S(\kappa)$ . These points form a surface in the 3-dimensional space of separation parameters, specified by the coordinates  $(\kappa, \zeta)$ . In the control parameter space  $\mathcal{H}$ , the points form a hypersurface  $\mathcal{H}_f$ , where

$$\mathcal{H}_f: S(u) = \zeta + (u - \kappa)^3 \cdot (u + 3\kappa), \quad \zeta \geq 0. \quad (4.2)$$

Comparison with (2.3) yields the parameter representation

$$\mathcal{H}_f: g_2 = 6\kappa^2, \quad g_3 = -8\kappa^3, \quad g_4 = 3\kappa^4 - \zeta. \quad (4.3)$$

Endpoints of  $\mathcal{H}_f$  are given by  $\zeta = 0$ , and they agree with the cusps of the bifurcation hypersurface  $\mathcal{H}$ . The identified  $\mathcal{H}_f$  is thus the familiar feature of the  $A_3$  glass transition singularity [17].

There is a special line  $\kappa = 0, \zeta \geq 0$  on  $\mathcal{H}_f$ . It is a scaling line which is obtained as cut of  $\mathcal{H}_f$  with the plane  $g_2 = 0$ . On this line, shown in Fig. 2 in dashed,  $S$  is constant up to fourth order correction terms:  $S = S_\zeta + u^4$ . This means that both inflection points coincide. The inset 1 in Fig. 2 shows the  $\varepsilon''$  versus  $u$ -curve for  $g_2 = 0, g_3 = 0, g_4 = -0.61$ . So the  $1/f$ -noise susceptibility plateau is limited on the low as well as on the high frequency side by susceptibility increases. The set of points in  $\mathcal{H}$ , where such behaviour is predicted, has dimensionality  $N - 2$ . Generically, a path  $T \rightarrow \mathbf{V}(T)$  will not cross this regime. Here and in the following typical parameter triples are indicated in Figs. 1–3 by squares with reference numbers, to be referred to as state numbers; the centre of the square is the parameter point. The corresponding  $\varepsilon''$  ( $\log \omega$ ) graph is shown in full close to the square.

The cuts of  $\mathcal{H}_f$  with the plane  $g_2 = 1$  are shown in Fig. 1 in dashed. These are straight lines with the parameter representation  $g_3 = \mp 4/(3\sqrt{6}), g_4 = 1/12 - \zeta, \kappa = \pm 1/\sqrt{6}$ . There the polynomial  $S(u)$  also has a minimum at  $u = u_0 = -2\kappa$  with  $S_0 = S(u_0) = \zeta - 27\kappa^4$ . For  $0 < \zeta < 27\kappa^4$  the minimum is negative. Thus there exists a zero  $u_-, S(u_-) = 0$ , with  $u_0 < u_- < \kappa$ . So one gets in a leading order approximation  $\varepsilon'' = 0$  for  $u < u_-$ . In this case the susceptibility spectrum has a typical behaviour relevant for  $1/f$ -noise near an  $A_3$  singularity as is shown in Fig. 1 for state 2 with  $g_2 = 1, g_3 = -0.544, g_4 = -0.527$ . The corresponding part of the second line with  $\kappa = -\sqrt{g_2}/6$  is not shown in Fig. 1; since (1.5) is violated there, it has not relevance for the dynamics. For  $\zeta > 27\kappa^4$  the susceptibility spectrum exhibits a minimum in addition to the  $1/f$ -noise plateau. It is located on the low frequency side of the plateau if  $g_3 < 0$  and on the high frequency side if  $g_3 > 0$ . This is shown in Fig. 1 for state 3 with  $g_2 = 1, g_3 = -0.544, g_4 = -0.804$  and for state 4 with  $g_2 = 1, g_3 = 0.544, g_4 = -0.804$ .

The relaxation patterns for states 3 and 4 are characteristic for  $A_4$ -behaviour; they cannot be found near a simple  $A_3$  singularity. Inset 3 shows a  $\beta$ -relaxation minimum, which is characteristic for states on the weak coupling side of an  $A_2$  fold hypersurface. The high frequency part of the spectra for states 2 and 3, i.e. the critical spectrum, is essentially the same. But it is not the simple power law spectrum  $\varepsilon'' \propto \omega^a$ , expected according to

(3.15) for the  $A_2$  singularity. The presence of an  $A_3$  singularity deforms the critical spectrum of the fold by adding an  $1/f$ -plateau. Viewing the states 2, 3 differently one can also say: the  $A_3$  singularity causes a  $1/f$  susceptibility plateau. But on the low frequency side the plateau spectrum exhibits the anomalies of a type  $B$  transition, a  $\beta$ -minimum appears upon crossing a fold hypersurface. Upon crossing the fold hypersurface with  $\xi > 0$  one also observes a type- $B$  transition. The typical  $\beta$ -minimum of the liquid spectrum disappears in the glass. Here only a critical spectrum  $\varepsilon'' \propto \omega^a$  is present, as shown for state 5 in Fig. 1 for  $g_2 = 1, g_3 = 0.544, g_4 = -0.527$ . This power law spectrum is shared for both states 4 and 5. But the low frequency liquid state spectrum does not show the simple von Schweidler power law  $\varepsilon'' \propto 1/\omega^b$ , expected for an  $A_2$  singularity. This part of the spectrum, which is also the high frequency part of the  $\alpha$ -relaxation peak, is distorted by the presence of an inaccessible  $A_3$  singularity. Upon decreasing the frequency  $\omega$ , the  $1/\omega^b$  spectrum develops an  $1/f$ -plateau, before it continues to increase up to the  $\alpha$ -peak maximum; the latter is not described by the present theory.

#### 4.2. Double minima

The low frequency spectra near a corner of the transition hypersurface  $\mathcal{D}_\xi$  exhibit a double peak [19]. Connected with these peaks are two minima. This pair of minima and the susceptibility peak between the minima are described by the present theory. The corner of the swallow tail has the parameter representation  $g_2 = 2\xi^2, g_3 = 0, g_4 = -\xi^4$ . The hypersurface with the larger form factor  $f_q^+ = f_q^c + h_q \cdot \rho^2 \cdot \delta f, \delta f = \xi = \sqrt{g_2}/2$ , terminates the one with the smaller form factor  $f_q^- = f_q^c - h_q \cdot \rho^2 \cdot \delta f$ . The pattern with the double minima occurs for the parameter region in Fig. 1 between the transition lines, below the corner for  $|g_3| < 4/(3\sqrt{6})$ . The hypersurface  $\mathcal{H}_f$  is the boundary of the double minima region, where one of the minima degenerates with the maximum of the  $\varepsilon''$  versus  $\log \omega$  curves to form a  $1/f$ -noise plateau. For  $g_3 < 0$  the low frequency minimum is deeper than the high frequency one, as shown in Fig. 1 for state 6 with  $g_2 = 1, g_3 = -0.230, g_4 = -0.508$ . For  $g_3 > 0$  the situation is reversed, as shown for state 7 with  $g_2 = 1, g_3 = 0.230, g_4 = -0.508$ . On the hypersurface  $g_3 = 0$  the minima have the same depth and the  $\varepsilon$  diagramm is rather symmetric. The insets in Fig. 1 for states 6 and 7 are completed schematically in dotted on the low frequency side, so that the reader can recognize the two peak structure of the  $\alpha - \beta$ -spectrum.

Suppose one crosses  $\mathcal{D}_\xi$  for  $g_3 > 0$ . One observes a type  $B$  transition with the high frequency  $\varepsilon''$ -minimum playing the role of the critical  $\beta$ -relaxation minimum. The spectrum changes as indicated in Fig. 1 by the transition from state 7 to state 8, where the latter is chosen for the parameters  $g_2 = 1, g_3 = 0.325, g_4 = -0.407$ . Both states share the critical spectrum. The whole spectrum below the critical minimum disappears upon crossing the fold. Both maxima including the minimum between them obey the  $\alpha$ -relaxation scaling. The transition is one with an  $\alpha$ -

spectrum split into an  $\alpha$ - $\alpha'$ -double peak [19]. The change of the spectrum upon crossing  $\mathcal{D}_\mathcal{E}$  for  $g_3 < 0$  is quite different. This is illustrated in Fig. 1 for transition from state 6 to state 9, where the latter refers to  $g_2 = 1$ ,  $g_3 = -0.325$ ,  $g_4 = -0.407$ . Here the low frequency minimum is relevant for the bifurcation. The spectra of states 6 and 9 share a maximum and the high frequency minimum. Both features appear as strong distortions of the critical spectrum for the  $\beta$ -relaxation of the considered transition. There is an ideal transition accompanied by a  $\gamma$ -peak [19].

States like 9, located in Fig. 1 between  $\mathcal{H}_f$  and the two pieces of  $\mathcal{D}_\mathcal{E}$ , show qualitatively the complete  $\alpha$ - $\beta$ -spectrum, which is characteristic for a state on the weak coupling side of an  $A_2$ -fold hypersurface. Crossing the hypersurface by moving from state 9 to 10, where the latter is chosen for  $g_2 = 1$ ,  $g_3 = 0$ ,  $g_4 = -0.100$ , one observes the spectral change due to an ideal glass transition.

#### 4.3. Linear log $\omega$ variations

The  $\varepsilon''$  versus  $\log \omega$  graphs for the  $\beta$  spectra near a simple  $A_2$  singularity are convex curves. On the glassy side of the bifurcation hypersurface they describe the crossover from  $\omega^1$  to  $\omega^a$  behaviour; so they increase monotonically as shown for states 5, 8 or 10 in Fig. 1. On the liquid side of the transition the curves describe the transition from a von Schweidler behaviour  $\omega^{-b}$  to critical relaxation  $\omega^a$  and so they exhibit a simple minimum. A qualitative distortion of those patterns is obtained if the curves exhibit an inflection point. Near such points the curves vary almost linearly. Let us identify such regions of linear log  $\omega$  variations outside the regions discussed above in Sects. 4.1., 4.2.. One has to identify points of inflections, given by  $S_{,uu}(u) = 0$ , i.e. points where

$$g_2 = 6 \cdot u^2. \quad (4.4)$$

The slopes  $\gamma$  of the diagrams are requested not to vanish:

$$\gamma = S_{,u}(u) \neq 0. \quad (4.5)$$

Obviously, such points occur only on the nontrivial side of the swallow tail  $g_2 \geq 0$ .

On the hypersurface  $g_2 = 0$  the points under discussion are given by  $u = 0$ . Hence one finds  $S_{,uuu}(u) = 0$  in addition to  $S_{,uu}(u) = 0$ ; the graphs approximate the linear behaviour not only in leading but even in next-to-leading order. Since  $S(u=0) = -g_4$ , only the points with  $g_4 \leq 0$  are candidates. For  $g_4 > 0$  the spectra exhibit the characteristic glass behaviour. This is shown in Fig. 2 for the state 11 with  $g_2 = 0$ ,  $g_3 = -0.838$ ,  $g_4 = 0.111$ . The same holds for all states with  $g_3 > 0$  above the fold line, as shown for state 12 with  $g_2 = 0$ ,  $g_3 = 0.838$ ,  $g_4 = -0.259$ . Here the inflection point occurs in a region not relevant for our dynamical discussion. The line  $g_4 = 0$ ,  $g_3 < 0$ , shown in Fig. 2 as doubly dashed one, separates the interesting region from the one with conventional behaviour. For the slope one gets  $\gamma = -g_3$ . The dashed line in Fig. 2 separates the region with  $\gamma > 0$  from that with  $\gamma < 0$ . For  $g_3 > 0$  the linear log  $\omega$  variation occurs on the

low frequency side of the minimum, which is the high frequency wing of the  $\alpha$ -peak. This is shown for state 13 with  $g_2 = 0$ ,  $g_3 = 0.733$ ,  $g_4 = -0.425$ . Upon crossing the fold, by moving from state 13 to 12, the whole anomaly gets lost. The critical spectrum for that transition, which is shared by states 12 and 13, is not influenced by the anomaly. For  $g_3 < 0$ ,  $g_4 < 0$  one gets the linear log  $\omega$  region with  $\gamma > 0$ . This is shown for the glass state 14 with  $g_2 = 0$ ,  $g_3 = -0.838$ ,  $g_4 = -0.259$  and for the liquid state 15 with  $g_2 = 0$ ,  $g_3 = -0.733$ ,  $g_4 = -0.425$ . Moving from state 15 to 14 one observes a type  $B$  transition which eliminates the wing of the  $\alpha$ -peak. Close to the line both states share the critical high frequency spectrum. The latter is not the simple  $\varepsilon'' \propto \omega^a$  power law, but it is deformed to a piece of linear log  $\omega$  variation.

Points of interest with  $g_2 > 0$  can be discussed for the cut  $g_2 = 1$ , shown in Fig. 1. Here the polynomial  $S(u)$  has two inflection points with  $u_\pm = \pm \sqrt{g_2/6}$ . There is the hypersurface  $\mathcal{H}_{\log}$  separating the region with  $S(u_\pm) < 0$  from that with  $S(u_\pm) > 0$ . It is given by the equation

$$\mathcal{H}_{\log}: g_4 = -\frac{3}{36} g_2^2 - g_3 \sqrt{\frac{g_2}{6}}. \quad (4.6)$$

It terminates at the cusp line; it is shown in double dashed in Fig. 1 for the cut with the  $g_2 = 1$  plane. States above the line do not show the linear log  $\omega$  behaviour as shown for state 16 with  $g_2 = 1$ ,  $g_3 = -0.812$ ,  $g_4 = 0.259$ . The same holds for all states above the fold line with  $\xi > 0$ , as shown for states 5, 8, 10 and 17, where the latter has coordinates  $g_2 = 1$ ,  $g_3 = 0.891$ ,  $g_4 = -0.878$ . For all states below  $\mathcal{H}_{\log}$  and above the fold line there is a region of linear log  $\omega$  variation with  $\gamma > 0$ . This is shown in Fig. 1 for state 18 with  $g_2 = 1$ ,  $g_3 = -0.891$ ,  $g_4 = 0.148$  and for state 19 with  $g_2 = 1$ ,  $g_3 = -0.891$ ,  $g_4 = -0.878$ . States below the fold line have two inflection points. One of them is intimately connected with the susceptibility minimum and so its existence does not appear as striking. The other inflection point causes a linear log  $\omega$  region with  $\gamma > 0$  for  $g_3 < 0$  or with  $\gamma < 0$  for  $g_3 > 0$ . This is shown in Fig. 1 for state 20 with  $g_2 = 1$ ,  $g_3 = -0.812$ ,  $g_4 = -0.961$  and for state 21 with  $g_2 = 1$ ,  $g_3 = 0.812$ ,  $g_4 = -0.961$  respectively. Moving from state 20 to 19 a type  $B$  transition occurs. The linear log  $\omega$  part is a deformation of the high frequency critical spectrum. For state 21 the linear log  $\omega$  part is a deformation of the high frequency  $\alpha$ -peak wing and therefore it gets lost if a type  $B$  transition to state 17 is considered.

For states with  $g_2 < 0$  the  $\varepsilon''(\log \omega)$  curves look similar to what one expects for a simple  $A_2$ -scenario. This is shown in Fig. 3 for the two glass spectra for state 22 with  $g_2 = -1$ ,  $g_3 = -4.686$ ,  $g_4 = -2.281$  and state 24 with  $g_2 = -1$ ,  $g_3 = 4.686$ ,  $g_4 = -2.281$  as well as for the two liquid spectra for state 23 with  $g_2 = -1$ ,  $g_3 = -3.943$ ,  $g_4 = -2.519$  and state 25 with  $g_2 = -1$ ,  $g_3 = 3.943$ ,  $g_4 = -2.519$ . There are deformations of the spectra, as is obvious from the complicated formula (3.12) for the critical decay.

A special type of deformation becomes obvious, if one considers the more sensitive  $\log \varepsilon''$  versus  $\log \omega$  diagrams,

which are shown in dashed in Fig. 3. There appear regions of linear  $\log \omega$  behaviour due to inflection points of the curves. They are obtained as solution of the equations  $S_{,u}^2 = 2 \cdot S \cdot S_{,uu}$ ,  $S_{,uuu} = 0$ . Such solutions exist for the cut in Fig. 3 for  $g_3 < 0$ ,  $g_4 < 0$  shown in double dashed and for the points below the bifurcation line for  $g_3 > 0$ . There appears a hypersurface described as

$$\mathcal{H}'_{\log} : g_4 = \frac{g_3^2}{4g_2}. \quad (4.7)$$

It is shown as double dashed parabola in Fig. 3. States below this parabola do not exhibit inflection points. States above the parabola exhibit two or one linear  $\log \omega$  behaviour (inflection points) as shown by the dashed inserts for states 22, 23, 25. For  $g_3 < 0$  the high frequency linear  $\log \omega$  region belongs to the critical spectrum of the type *B* transition through the fold; it is shared by the states 22 and 23. For  $g_3 > 0$ , the linear  $\log \omega$  part is a deformation of the high frequency  $\alpha$ -peak tail. Therefore it gets lost upon crossing the fold line by moving from state 25 to 24. On  $\mathcal{H}'_{\log}$  two inflection points coincide and thus the linear  $\log \omega$  behaviour hods in leading as well as in next to leading order for the  $\log(\varepsilon'')$ - $\log \omega$  diagram. This is shown for state 26 with  $g_2 = -1$ ,  $g_3 = -3.746$ ,  $g_4 = -3.508$  and state 27 with  $g_2 = -1$ ,  $g_3 = 3.746$ ,  $g_4 = -3.508$ . In the former case the anomaly occurs on the high frequency part of the  $\beta$ -relaxation minimum, and in the latter case on the low frequency one.

## 5. Applications

In order to compare the previous theory with measured spectra the various parameters have to be determined. The three parameters  $f_c$ ,  $\varepsilon_c$  and  $t_1$  set the scales, and can be determined once the shape of  $\varepsilon$  has been fixed. The latter is strongly influenced by the values of the three separation parameters  $g_2$ ,  $g_4$ , as illustrated in Figs. 1–3. To find the precise values for these parameters, which will fit a particular loss curve, one must extract some information from the experimental data. In case the spectrum has a double minimum one can use the relative heights of the three extrema in  $\varepsilon''$  and the distance between the minima to determine  $g_2$ ,  $g_3$  and  $g_4$ . This was done in the following way. Three extremal points are obtained when the equation

$$S_{,u}(u) = 4 \cdot u^3 - 2g_2 \cdot u - g_3 = 0 \quad (5.1)$$

has three real roots. Let us introduce the scaled parameters  $\hat{g}_2 = 1$ ,  $\hat{g}_3$  and  $\hat{g}_4$  and the scaling parameters  $s = \sqrt{g_2}$ . Then one can express the roots in terms of  $s$  and the angles  $\theta_1$ ,  $0 \leq \theta_1 \leq \pi/3$  and  $\theta_{2,3} = \theta_1 \pm 2\pi/3$

$$u_{1, \min} = s \cdot \left(\frac{2}{3}\right)^{1/2} \cdot \cos \theta_1 \quad (5.2)$$

$$u_{2, \min} = s \cdot \left(\frac{2}{3}\right)^{1/2} \cdot \cos \theta_2 = -s \cdot \left(\frac{1}{6}\right)^{1/2} \cdot (\cos \theta_1 + \sqrt{3} \cdot \sin \theta_1) \quad (5.3)$$

$$u_{3, \min} = s \cdot \left(\frac{2}{3}\right)^{1/2} \cdot \cos \theta_3 = -s \cdot \left(\frac{1}{6}\right)^{1/2} \cdot (\cos \theta_1 - \sqrt{3} \cdot \sin \theta_1) \quad (5.4)$$

where  $u_{1, \min}$  denotes the high frequency minimum and  $u_{2, \min}$  the low frequency one. The angle  $\theta_1$  can be calculated from the experimentally determined parameters

$$r_1 = \left(\frac{\varepsilon''_{1, \min}}{\varepsilon''_{\max}}\right)^2, \quad r_2 = \left(\frac{\varepsilon''_{2, \min}}{\varepsilon''_{\max}}\right)^2, \quad (5.5)$$

through the equation

$$\left(1 + \frac{x^2}{3}\right) \cdot \cos^8 \theta_1 - (1 + x^2) \cdot \cos^6 \theta_1 + x^2 \cdot \cos^4 \theta_1 + \left(\frac{1}{8} - \frac{x^2}{3}\right) \cdot \cos^2 \theta_1 + \frac{1}{64} = 0, \quad (5.6)$$

where  $x = 1 - 2 \cdot (r_1 - r_2) / (1 - r_2)$ . This equation can be solved numerically to obtain  $\cos \theta_1$ . This value then determines the scaled parameters via

$$\hat{g}_3 = \frac{2}{3} \cdot (4 \cos^3 \theta_1 - 3 \cos \theta_1) \quad (5.7)$$

$$\begin{aligned} \hat{g}_4 &= \frac{2}{3(1-r_2)} \cdot [\cos^2 \theta_2 \cdot (1 - 2 \cos^2 \theta_2) \\ &\quad - r_2 \cos^2 \theta_3 \cdot (1 - \cos^2 \theta_3)] \\ &= \frac{2}{3(1-r_2)} \cdot [\cos^2 \theta_1 \cdot (1 - 2 \cos^2 \theta_1) \\ &\quad - r_1 \cos^2 \theta_3 \cdot (1 - \cos^2 \theta_3)]. \end{aligned} \quad (5.8)$$

The limiting cases where  $r_1 = 1$  or  $r_2 = 1$  correspond to horizontal inflexion points in  $\varepsilon''$  located at  $\theta_1 = \pi/3$  and  $\theta_1 = 0$  respectively. The scaling factor  $s$  finally was obtained from the position of the minima  $\omega_{1, \min}$  and  $\omega_{2, \min}$  through

$$s = \frac{1}{\ln(\omega_{1, \min}) - \ln(\omega_{2, \min})} \int_{\hat{u}_{2, \min}}^{\hat{u}_{1, \min}} \frac{du}{\sqrt{u^4 - u^2 - \hat{g}_3 \cdot u - \hat{g}_4}}, \quad (5.9)$$

where  $\hat{u}_{i, \min} = u_{i, \min} / s$ ,  $i = 1, 2$ . This way of determining the parameters worked very well in the cases studied below. In practice the separation between the minima can be slightly adjusted to get the best fit. The scales  $\varepsilon_c$  and  $t_1$  were then fixed from the experimental values for one of the minima. In general these parameters may have some regular dependence on temperature.

In case there is a linear variation of  $\varepsilon''$  with  $\ln \omega$  we can use the slope  $\gamma$  to determine one parameter. In cases where there is also a minimum the value of this is used to fix a second parameter. One finds

$$g_3 = \frac{4\gamma}{\pi\varepsilon_c} \mp \frac{4g_2^{3/2}}{3\sqrt{6}}, \quad (5.10)$$

and

$$g_4 = u_{\min}^4 - g_2 \cdot u_{\min}^2 - g_3 \cdot u_{\min} - \left( \frac{2\varepsilon''_{\min}}{\pi\varepsilon_c} \right)^2. \quad (5.11)$$

Here the minus sign in (5.10) must be used if the linear region is on the high frequency side of the minimum and the plus sign in the other case. Notice that  $\gamma$  is the slope with respect to  $\ln\omega$ , i.e. the natural logarithm is used. The parameter  $g_2$  has to be used a parameter to get the best fit. For  $\varepsilon_c$  one can use the same value as obtained above from the case of a double minimum, provided this parameter has only a slight temperature dependence. In case that there is only one minimum in the spectrum with no other obvious structure one has to use both  $g_2$  and  $g_3$  as free parameters and determine  $g_4$  from (5.11).

It was shown [13] that the dielectric functions measured by Scott et al. [20] for PCTFE with 44% crystallinity could be interpreted well with the MCT results for an  $A_3$  glass transition singularity. This is certainly not possible for the data obtained for 80% crystallinity [20]. Figure 4a-c reproduce the experimental findings and fits by the results of the preceding theory. The separation parameters were determined as explained above and are noted in the figure captions. The data for  $T=200$  °C exemplify linear  $\log f$  variations over a window of 2.5 decades on the high frequency side of the minimum and the fit corresponds to state 15 in Fig. 2. The spectrum for  $T=175$  °C exhibits a double minimum as in state 6 in Fig. 1. There is also the high frequency tail of the low frequency  $\alpha$  peak; its maximum occurs below  $10^{-2}$  Hz. The spectrum for  $T=150$  °C exhibits a  $1/f$ -noise region over a frequency interval as large as 4 decades and the system is close to state 1 in Fig. 2. The corresponding fit curves

shown as solid lines Fig. 4a-c demonstrate an increasing of fit accuracy by lowering the temperature. Especially the fit for  $T=150$  (Fig. 4c) is able to reproduce more than 50% of the low frequency side of the  $\beta$ -peak, located close to  $10^7$  Hz. In the case of  $T=175$  °C (Fig. 4b) the above described parameter determination fixes only the relative heights of the three extrema and the positions of both minima. The position of the maximum as well as the slopes of the curves at the low frequency side of the low frequency minimum and the high frequency side of the high frequency minimum are nontrivial outcomings of the theory. The parameter  $\varepsilon_c$  given in the figure captions was found to have some temperature dependence. The values are rather sensitive to the precise choice of the separation parameters and therefore rather uncertain. The same holds for the time scale  $t_1$  and its variation is probably not significant.

The data for a crystallinity of 73% can partly be fitted by the formulae for an  $A_3$  singularity, as is exemplified by the dashed lines in Fig. 5a, b for  $T=148$  °C and  $T=174$  °C, respectively. Within this frame, the low frequency  $\alpha$ -peak wing is described as white noise, like for a conventional  $\alpha$  peak at an  $A_2$  singularity; compare state 9 in Fig. 1. The stretching of the  $\alpha$  peak shown in Fig. 5a for frequencies below  $10^2$  Hz and in Fig. 5b for frequencies below  $10^3$  Hz cannot be understood within a simple  $A_2$  or  $A_3$  scenario. The spectra can be fitted reasonably over a window of 6 decades by our formulae for an  $A_4$  singularity as shown by the full curves in Fig. 5a, b. Again at the lower temperature  $T=148$  °C (Fig. 5a) the fit reproduces the low frequency side of the  $\beta$ -peak better than for the higher temperature  $T=174$  °C. In this case the  $A_4$  fit proposes additional structures at lower frequencies outside the experimental frequency window. But these

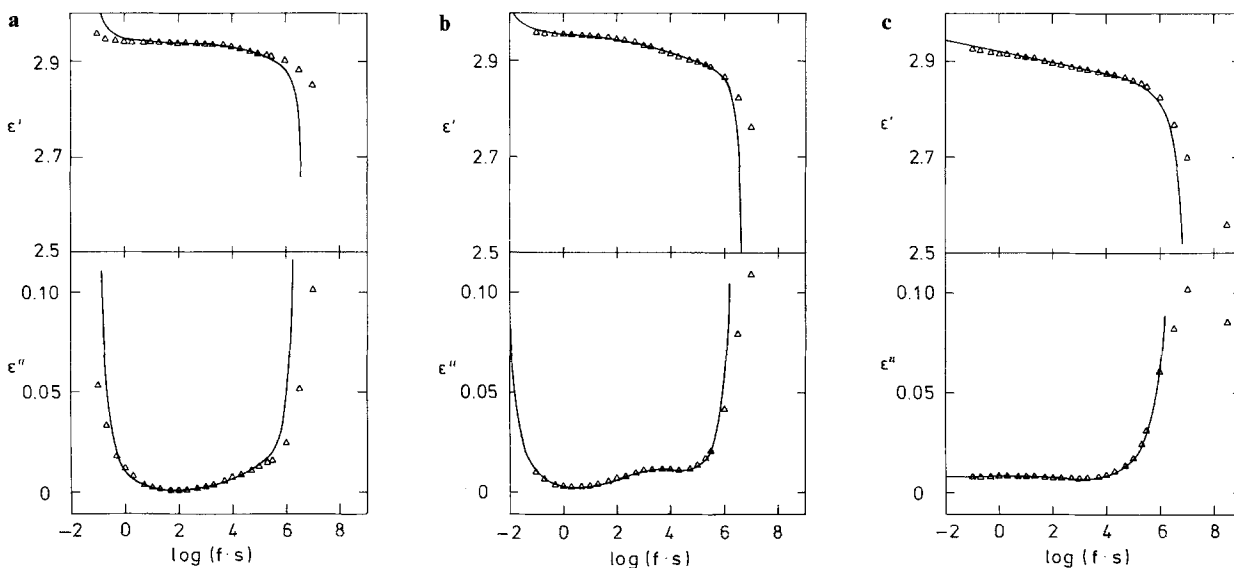


**Fig. 4.** a Dielectric constant  $\varepsilon = \varepsilon' + i\varepsilon''$  as function of  $\log f$  for PCTFE with 80% crystallinity at  $T=200$  °C from [20]; Full lines:  $A_4$  fit with parameters  $g_2=0$ ,  $g_3=-0.0584$ ,  $g_4=-0.00108$  and scales  $f_c=2.92$ ,  $\varepsilon_c=0.0663$ ,  $t_1=1.63 \cdot 10^{-7}$  s. b Same as Fig. 4a but  $T=175$  °C and fit parameters  $g_2=0.08926$ ,  $g_3=-0.009414$ ,

$g_4=-0.004359$ ,  $f_c=2.93$ ,  $\varepsilon_c=0.1103$ ,  $t_1=1.832 \cdot 10^{-7}$  s. c Same as in Fig. 4a, b but  $T=150$  °C and fit parameters  $g_2=0.019633$ ,  $g_3=-0.002834$ ,  $g_4=-0.0004449$ ,  $f_c=2.91$ ,  $\varepsilon_c=0.256$ ,  $t_1=6.67 \cdot 10^{-8}$  s

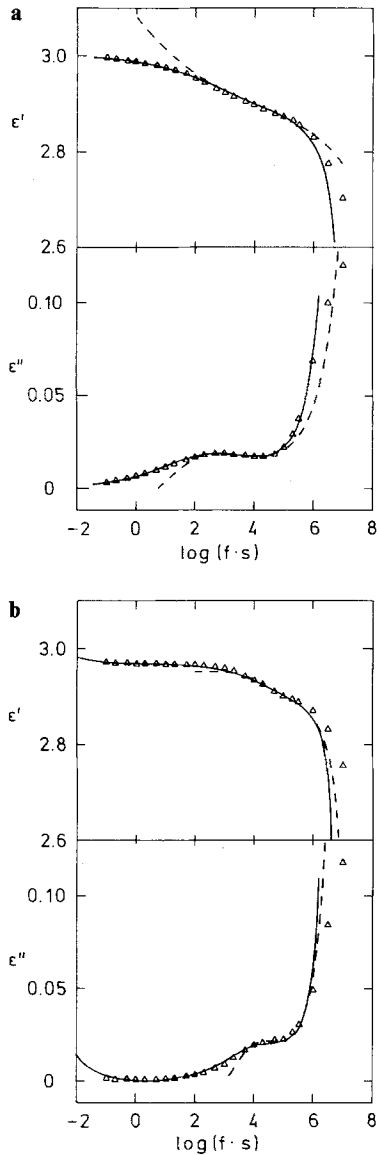


**Fig. 5.** **a**  $\epsilon'$  and  $\epsilon''$  as functions of  $\log f$  for PCTFE with 73% crystallinity and  $T=148^\circ\text{C}$  from [20]; solid line:  $A_4$  fit with parameters  $g_2=0.05423$ ,  $g_3=-0.00376$ ,  $g_4=-0.00138$ ,  $f_c=2.924$ ,  $\epsilon_c=0.318$ ,  $t_1=7.24\cdot 10^{-8}$  s; dashed line:  $A_3$  fit with parameters  $g_2=2.9667\cdot 10^{-4}$ ,  $g_3=-1.1986\cdot 10^{-5}$ . **b** Same as in Fig. 5a but  $T=174^\circ\text{C}$ ; solid line:  $A_4$  fit with parameters  $g_2=0.09443$ ,  $g_3=-0.02071$ ,  $g_4=-0.007219$ ,  $f_c=2.93$ ,  $\epsilon_c=0.1485$ ,  $t_1=8.77\cdot 10^{-8}$  s; dashed line:  $A_3$  fit with parameters  $g_2=0$ ,  $g_3=-3\cdot 10^{-4}$

different structures leave the fitted part of the spectrum unchanged. Thus we cannot decide from this fit whether the system corresponds to state 6 or state 9 in Fig. 1.

Several studies of the dielectric loss in linear polyamides with varying degrees of crystallinity as well as varying water content have been made [21–24]. It was recognized that the spectra of these systems have a rather complex structure which does not satisfy the time temperature superposition principle for instance [22]. For low frequencies there is a strong loss region, which could not be attributed to d–c conduction [21], [24]. For temperatures above  $80^\circ\text{C}$  there appears a loss maximum for

higher frequencies. Some characteristic results for nylon 610, with a high degree of crystallinity, by Baker and Yager [21] are shown in Fig. 6a–d for four temperatures. For the highest frequencies  $f\approx 10^8$  Hz there is some indication of a minimum, and the spectra for  $T=120^\circ\text{C}$  and  $T=100^\circ\text{C}$  would then have the characteristic double minimum structure, as is shown for states 6 or 7 in Fig. 1. For  $T=79^\circ\text{C}$  there is a clear inflection point at  $f\approx 10^4$  Hz while for  $T=60^\circ\text{C}$  there is a region of almost linear variation in  $\log f$  over three decades; but opposed to the example shown in Fig. 4a, now the linear region is on the low frequency side of the minimum. These features correspond to state 4 in Fig. 1 and state 13 in Fig. 2 respectively. The full curves in Fig. 6a–d show the theoretical results for both  $\epsilon'$  and  $\epsilon''$  using the  $A_4$  scenario. Here the position and height of the high frequency minimum were adjusted to get a good overall fit. The parameters used are given in the figure captions, and give a smooth path from state 6 over states 7 and 4 to state 21 approaching the plane  $g_2=0$ . Due to the uncertainty in the location and height of the minimum, there are some reservations in the values obtained for  $\epsilon_c$  and  $t_1$ . The former was found to be essentially constant with  $\epsilon_c=16$ , and this value was used to obtain the result in Fig. 6d. For  $t_1$  we found true microscopic values, which decrease somewhat with decreasing temperature. The parameter  $f_c$  shows a gradual increase with temperature. The loss data by Boyd [22] and Curtis [24] show similar features and can also be fitted within an  $A_4$ -scenario.

For lower temperatures the loss spectra become constant over a large frequency interval. This  $1/f$  noise feature in the spectra is further illustrated in Fig. 7, where we show the spectrum  $\phi''(f)=\epsilon''/f$  versus frequency  $f$  for the three temperatures  $T=120^\circ\text{C}$ ,  $60^\circ\text{C}$  and  $27.6^\circ\text{C}$ . In this form the data show a clear  $1/f$  noise behaviour even for  $T=120^\circ\text{C}$ , where the structure in Fig. 6a degenerates to some wiggling in Fig. 7. The full curves are the theoretical results corresponding to the results in Fig. 6. For  $T=27.6^\circ\text{C}$  the experimental data show a perfect linear behaviour over five decades of frequency variation. The full curve through the data points was obtained with parameters  $g_2=g_3=0$  and  $g_4$  adjusted to get the correct level. The linear region in the theoretical results for  $T=27.6^\circ\text{C}$  continues some 15 decades more on the low frequency side, i.e. there is around 30 decades of  $1/f$  noise for this temperature. Eventually there is a cross over for both low and high frequencies due to the  $\alpha$ - and  $\beta$ -peaks respectively. Clearly by approaching the swallow tail singularity in Fig. 2 along the line  $g_3=0$  the  $1/f$  noise region extends further and further as can also be inferred from the scaling property in (2.14). Figure 7 shows that the detailed structure in  $\epsilon''$  is not revealed in this kind of plot. The reason is that  $\epsilon$  in (2.16), (2.17) is given by a slowly varying function of frequency  $f$ , and this is rather constant in comparison to the factor  $1/f$  used to obtain  $\phi''$ . Therefore to reveal deviations from strict  $1/f$  noise one should rather plot the susceptibility spectra. Recent  $1/f$  noise spectra  $S_v(f)$  of voltage fluctuations in thick-film resistors were converted into susceptibility spectra  $f\cdot S_v(f)$  [25]. The results were very similar to the dielectric spectra for nylon 610 shown in

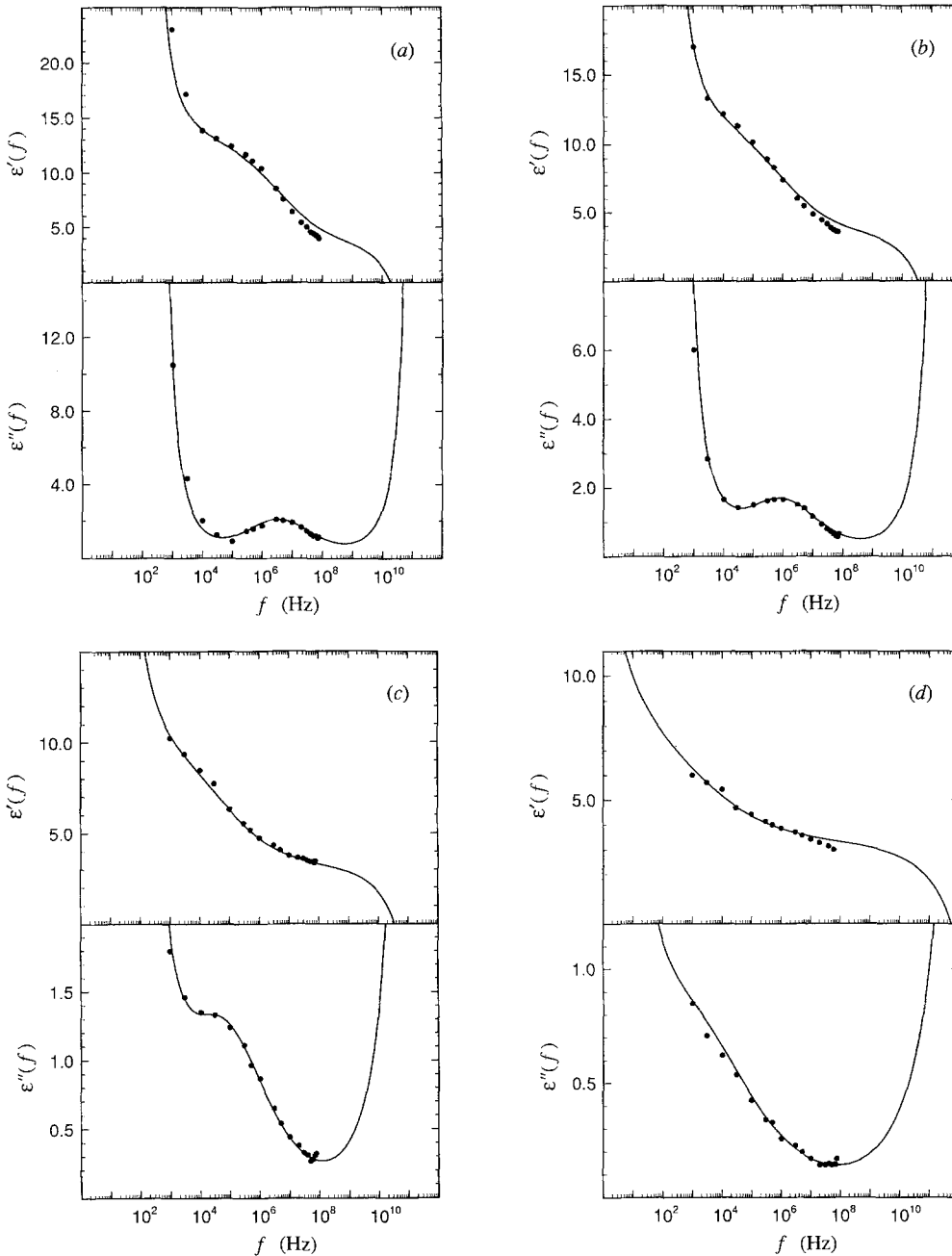


**Fig. 6.** **a**  $\varepsilon''$  and  $\varepsilon'$  versus frequency  $f$  for nylon 610 at  $T=120^\circ\text{C}$  from [21]; lines:  $A_4$  fits with parameters  $g_2=0.1403$ ,  $g_3=0.00153$ ,  $g_4=-0.00623$  and scales  $f_c=8.3$ ,  $\varepsilon_c=16.95$ ,  $t_1=8.77\cdot 10^{-13}$  s. **b** Same as in Fig. 6a but  $T=100^\circ\text{C}$ . Lines:  $A_4$  fits with parameters  $g_2=0.1034$ ,  $g_3=0.0059$ ,  $g_4=-0.00445$  and scales  $f_c=7.4$ ,  $\varepsilon_c=15.97$ ,  $t_1=4.52\cdot 10^{-13}$  s. **c** Same as in Fig. 6a but  $T=79^\circ\text{C}$ .

Lines:  $A_4$  fits with parameters  $g_2=0.068$ ,  $g_3=0.00962$ ,  $g_4=-0.00321$  and scales  $f_c=6.3$ ,  $\varepsilon_c=14.16$ ,  $t_1=4.05\cdot 10^{-13}$  s. **d** Same as in Fig. 6a but  $T=60^\circ\text{C}$ . Lines:  $A_4$  fits with parameters  $g_2=0.010$ ,  $g_3=0.00712$ ,  $g_4=-0.000842$  and scales  $f_c=5.5$ ,  $\varepsilon_c=16$ ,  $t_1=1.46\cdot 10^{-14}$  s

Fig. 6. A possible connection between slow relaxation in disordered systems and  $1/f$  noise has been suggested before [26–28], but has still to be investigated further [29].

Another system which shows the characteristic double minimum is polyoxymethylene (delrin) [30]. The experimental loss data by Ishida et al. are shown in Fig. 8 together with the  $A_4$  fits as full lines. In this case the double minimum is observed for the two highest temperatures while for the lower temperature there is a rather broad structureless minimum. The latter corresponds to

negative values of  $g_2$  as given in the figure captions. To obtain these two curves both  $g_2$  and  $g_3$  were used as free parameters while  $g_4$  was determined from (5.11) with  $\varepsilon_c=0.0965$ . For  $T=45.5^\circ\text{C}$  the parameters are rather close to the double dashed parabola in Fig. 3, i.e.  $\log \varepsilon''$  depends linearly on  $\log \omega$ . The rise in  $\varepsilon''$  at lower frequencies was in this case attributed to ionic conduction [30], and if this contribution is subtracted one cannot exclude that the spectra would look more like states 9 or 16 in Fig. 1.

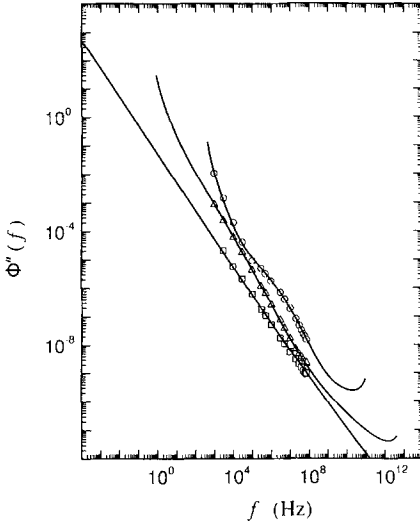


**Fig. 7.** The spectrum  $\phi'' = \epsilon''/f$  versus frequency  $f$  in a log-log plot for loss data obtained in [21] for nylon 610. circles:  $T=120^\circ\text{C}$ , triangles:  $T=60^\circ\text{C}$  and squares:  $T=27.6^\circ\text{C}$ . The lines are fits within the  $A_4$  scenario. For  $T=120^\circ\text{C}$  and  $60^\circ\text{C}$  the parameters are given in Fig. 6a and 6d respectively. The curve for  $T=27.6^\circ\text{C}$  was obtained with parameters  $g_2=0$ ,  $g_3=0$ ,  $g_4=-4.28 \cdot 10^{-6}$

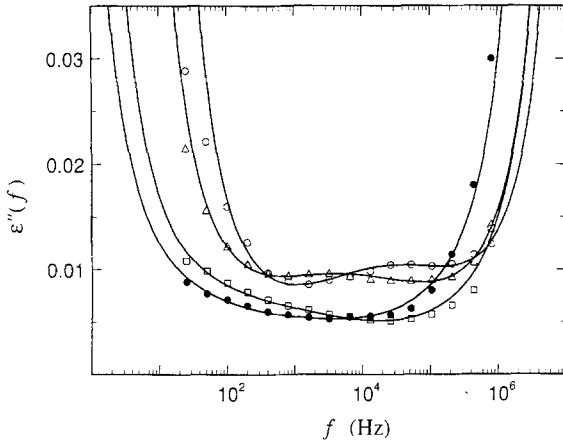


**Fig. 8.** Dielectric loss data for delrin from [30]. The lines are  $A_4$  fits. Open circles:  $T=68.5^\circ\text{C}$ ,  $g_2=5.57 \cdot 10^{-2}$ ,  $g_3=-4.66 \cdot 10^{-3}$ ,  $g_4=-5.03 \cdot 10^{-3}$ , scales:  $\epsilon_c=0.093$ ,  $t_1=4.83 \cdot 10^{-9}$  s; triangles:  $T=62^\circ\text{C}$ ,  $g_2=3.82 \cdot 10^{-2}$ ,  $g_3=1.53 \cdot 10^{-3}$ ,  $g_4=-3.74 \cdot 10^{-3}$ , scales:  $\epsilon_c=0.1$ ,  $t_1=6.36 \cdot 10^{-9}$  s; squares:  $T=45.5^\circ\text{C}$ ,  $g_2=-2 \cdot 10^{-2}$ ,  $g_3=9 \cdot 10^{-3}$ ,  $g_4=-1.75 \cdot 10^{-3}$ , scales:  $\epsilon_c=0.0965$ ,  $t_1=6.43 \cdot 10^{-9}$  s; filled circles:  $T=29.5^\circ\text{C}$ ,  $g_2=-4 \cdot 10^{-2}$ ,  $g_3=5 \cdot 10^{-3}$ ,  $g_4=-1.37 \cdot 10^{-3}$ , scales:  $\epsilon_c=0.0965$ ,  $t_1=1.63 \cdot 10^{-8}$  s

The  $\beta$ -relaxation spectra for parameters close to inner points of the bifurcation hypersurface  $\mathcal{D}_\beta$  are specified by the so called exponent parameter  $\lambda$ , where  $1/2 \leq \lambda < 1$ . The boundary points of  $\mathcal{D}_\beta$ , given by  $A_1$  singularities with  $l \geq 3$ , are characterized by  $\lambda \rightarrow 1$  [3].  $A_2$  spectra, fitted with a large  $\lambda$  are therefore disturbed by a nearby cuspid singularity with index  $l \geq 3$ . In such a case it might be more reasonable to explain the data by the asymptotic formulae valid for  $A_1$  singularities with  $l \geq 3$ . If an  $A_2$  pattern is observed to occur near an  $A_1$ ,  $l \geq 3$ , it might be possible to use the asymptotic formulae of the present

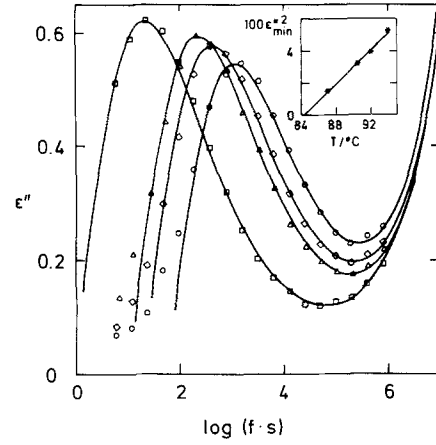


**Fig. 9.**  $\epsilon''$  as function of  $\log f$  for PEOB-I from [31]. The lines are  $A_3$  fits. Circles:  $T=94^\circ\text{C}$ ,  $g_2=2.62 \cdot 10^{-3}$ ,  $g_3=-3.68 \cdot 10^{-5}$ , scales:  $\epsilon_c=43.87$ ,  $t_1=4.45 \cdot 10^{-10}$  s; spades:  $T=92^\circ\text{C}$ ,  $g_2=2.424 \cdot 10^{-3}$ ,  $g_3=-2.90 \cdot 10^{-5}$ , scales:  $\epsilon_c=50.95$ ,  $t_1=2.19 \cdot 10^{-10}$  s; triangles:  $T=90.5^\circ\text{C}$ ,  $g_2=2.43 \cdot 10^{-3}$ ,  $g_3=-2.75 \cdot 10^{-5}$ , scales:  $\epsilon_c=53.3$ ,  $t_1=1.46 \cdot 10^{-10}$  s; squares:  $T=87^\circ\text{C}$ ,  $g_2=2.28 \cdot 10^{-3}$ ,  $g_3=-2.255 \cdot 10^{-5}$ , scales:  $\epsilon_c=59.93$ ,  $t_1=1.83 \cdot 10^{-10}$  s; insert: squared height of the minimum of  $\epsilon''$  versus temperature

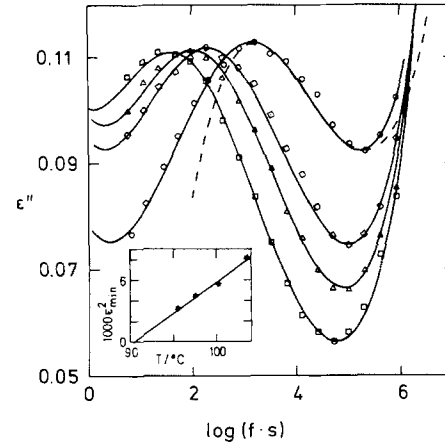


**Fig. 10.**  $\epsilon''$  as function of  $\log f$  for PEOB-IV from [31]. The lines are  $A_4$  fits. Circles:  $T=103.4^\circ\text{C}$ ,  $g_2=3.75 \cdot 10^{-2}$ ,  $g_3=-6.55 \cdot 10^{-4}$ ,  $g_4=-7.98 \cdot 10^{-4}$ , scales:  $\epsilon_c=2.54$ ,  $t_1=1.57 \cdot 10^{-9}$  s; spades:  $T=100.2^\circ\text{C}$ ,  $g_2=3.86 \cdot 10^{-2}$ ,  $g_3=7.57 \cdot 10^{-4}$ ,  $g_4=-8.64 \cdot 10^{-4}$ , scales:  $\epsilon_c=2.42$ ,  $t_1=2.25 \cdot 10^{-9}$  s; triangles:  $T=97.5^\circ\text{C}$ ,  $g_2=4.11 \cdot 10^{-2}$ ,  $g_3=1.42 \cdot 10^{-3}$ ,  $g_4=-9.84 \cdot 10^{-4}$ , scales:  $\epsilon_c=2.25$ ,  $t_1=3.30 \cdot 10^{-9}$  s; squares:  $T=95.5^\circ\text{C}$ ,  $g_2=4.31 \cdot 10^{-2}$ ,  $g_3=2.06 \cdot 10^{-3}$ ,  $g_4=-1.06 \cdot 10^{-3}$ , scales:  $\epsilon_c=2.15$ ,  $t_1=4.05 \cdot 10^{-9}$  s; insert: squared height of the minimum of  $\epsilon''$  versus temperature

paper to describe not only the  $\beta$  relaxation minimum but also the  $\alpha$  resonance, as demonstrated in Fig. 5. These observations are the motivation to reconsider the previous discussion [12], [13] of the PET and PEOB dielectric loss data published by Ishida et al. [31]. Figures 9, 10 demonstrate indeed, that the previous discussion can be extended to incorporate the  $\alpha$  peaks for the amorphous polymer PEOB-I (0% crystallinity) provided one uses the  $A_3$  results and for PEOB-IV (38% crystallinity) provided one uses the  $A_4$  results.

The PEOB-I data in Fig. 9 show that the  $A_3$  curves (solid lines) describe the loss spectra including the  $\alpha$ -maximum. The lowest 30% of the low frequency part of this maximum does not lie on the theoretical curves. This is not surprising since within the  $A_3$  theory all spectra exhibit a nonanalyticity:  $\varepsilon''$  becomes zero at a nonzero frequency. So in the vicinity of this point every experimental curve will differ from the leading order theoretical prediction. An interesting argument for the applicability of the  $A_3$  scenario for PEOB-I is the calculation of the singularity point  $T_c$  via the scaling relation  $\varepsilon''_{\min}(T) \sim (T - T_c)$  which comes from the scaling properties near an  $A_2$  singularity (cf. [13], see insert in Fig. 9) and a comparison with the theoretical prediction. This prediction comes from the found approximate linear temperature dependence of the two control parameters  $g_2(T)$ ,  $g_3(T)$ :

$$g_2(T) = (2.62 + 0.049 \cdot (T/\text{°C} - 94)) \cdot 10^{-3} \quad (5.12)$$

$$g_3(T) = (-3.68 + 0.204 \cdot (94 - T/\text{°C})) \cdot 10^{-3} \quad (5.13)$$

Equations (5.12), (5.13) are the result of the best fits in Fig. 9. Then one can calculate the temperature  $T_c^{\text{theor}}$  where the path (5.12), (5.13) crosses the critical hypersurface  $g_3 = -(g_2/3)^{3/2}$ . One obtains:

$$T_c^{\text{theor}} = 85.8 \text{ °C}. \quad (5.14)$$

It is non trivial, that this value is rather close to the value  $T_c = 84.4 \text{ °C}$  [13]. The control parameters are obtained by best fitting in a two-dimensional control parameter space with some bifurcation line in it. The value  $T_c$  is obtained using variations of spectra with one physical control parameter. Moreover this result confirms that although the loss curves near an  $A_2$  singularity can be strongly disturbed by the additional vicinity to an  $A_3$  singularity, the transition itself remains as an  $A_2$  transition and thus some scaling properties, obtained for  $A_2$  transitions, remain.

In Fig. 10 we show the PEOB-IV data. The  $A_3$  scenario is not able to describe the  $\alpha$  peaks, as is shown for one temperature by the dashed line. However the  $A_4$  scenario easily describes all experimental points. It is a result of a best fit in a three-dimensional control parameter space. The fits suggest, that there might be an additional maximum at frequencies lower than 10 Hz. We find, as in the previous case, a linear temperature dependence of the control parameters:

$$g_i = a_i \cdot T + b_i \quad (5.15)$$

$$\begin{aligned} a_2 &= -7.1 \cdot 10^{-4} & b_2 &= 1.1 \cdot 10^{-1} \\ a_3 &= -3.4 \cdot 10^{-4} & b_3 &= 3.4 \cdot 10^{-2} \\ a_4 &= 3.3 \cdot 10^{-5} & b_4 &= -4.2 \cdot 10^{-3}. \end{aligned} \quad (5.16)$$

Using these relations one can determine the theoretical prediction of the transition temperature  $T_c^{\text{theor}}$  as crossing point of the path (5.15) with the critical bifurcation surface described in 3.1.. Again the estimation

$$T_c^{\text{theor}} = 88.9 \text{ °C} \quad (5.17)$$

is rather close to the one from the zero,  $T_c = 90.4 \text{ °C}$  [13], of the  $\varepsilon''^2$  versus  $T$  curve.

The analysis for PET-I (5% crystallinity) and PET-IV (51% crystallinity) with both  $A_3$  and  $A_4$  predictions brought out no extension of the earlier  $\beta$ -minimum fit [13]; i.e. the  $\alpha$  peak could not be included in the analysis. This holds even though the PET data look rather similar to the PEOB ones.

## 6. Conclusions

Some comment shall be added to specify the perspective of the preceding calculations and data fittings. The MCT can be viewed on three levels. It can be considered *i*) as a first principle approximation approach towards the dynamics of a many particle system, *ii*) as a well defined mathematical model for a non-linear dynamics and *iii*) as a phenomenological theory for the interpretation of stretched relaxation spectra of complex systems. So far the microscopic approach has been worked out only for simple liquids and simple binary mixtures. One understands, that in those cases the theory deals primarily with cage effects and backflow phenomena as well as with activated processes. It is understood, that effects responsible for the formation of net-work glasses are ignored. These effects will presumably be essential for the understanding of glassy relaxation in associated liquids and systems with covalent bondings. Quantitative application of the simple liquid theory has been made only for the discussion of colloid dynamics [14]. Obviously complex systems like polymers are outside the scope of the microscopic theory at present, even though some impressive progress has recently been made [32], [33].

The microscopic theory yields Eqs. (1.1)–(1.3) and these equations define a precise mathematical model. It is worthwhile to study this model regardless of its motivation, since it leads to rather non-trivial results and since it has a considerable predictive power. This attitude was taken in the present paper. Let us emphasize, that the basic Eqs. (1.1)–(1.3) are regular. They do not anticipate any glass transition effects or fractal structures. The equations produce spontaneous singularities by way of bifurcations. The slow dynamics for these bifurcations is novel. A major part of the MCT concerns the study of the mathematical details of the correlation functions near the glass transition singularities. The results imply various fractal decay laws and logarithmic decay patterns, which explain stretching quite naturally. Working out of the mathematical details is an obvious necessity, if one wants to decide, whether or not the MCT is of any relevance for the interpretation of experiments. The analysis brings out, that many relaxation features near glass transition singularities, in particular the spectral shapes in the  $\beta$  regime, merely reflect the topology of a bifurcation hypersurface. Therefore these results are stable with respect to extensions of the theory. If ever a microscopic MCT for polymers can be established, it will also contain those singularities discussed e.g. in the present paper. It appears as a non-trivial outcome of the theory, that is establishes a well defined picture for glassy relaxation, which is shared

say between a hard spherical colloidal suspension and a polymer of high molecular weight. It is that subtle mathematical finding which makes it legitimate to compare results as derived in this paper with loss data of polymers.

Originally, the MCT was developed in order to study the ideal ergodic to non-ergodic transition for simple liquids or for particles moving in a random potential. The underlying singularity was an  $A_2$  singularity or a distortion thereof. The transition points are located on a hypersurface  $\mathcal{H}$  in the control parameter space. This is the most important case, since moving the system on a path  $C: T \rightarrow \mathbf{V}(T)$  by changing a single control parameter like the temperature  $T$ , one will (in the ideal case considered here) generically hit a singularity  $\mathbf{V}_c \in \mathcal{H}$  for a certain critical temperature  $T_c: \mathbf{V}(T_c) = \mathbf{V}_c$ . The range of validity of the asymptotic formulae for  $\mathbf{V} \sim \mathbf{V}_c$  should expand for  $(T - T_c) \rightarrow 0$ . It is quite evident, however, that relaxation spectra of polymers are often too complicated to be compatible with the simple  $A_2$  scenario. Often one observes  $\log(t)$ -behaviour for the time dependence or nearly  $1/f$ -noise plateaus. This is expected for  $A_l$  singularities with  $l \geq 3$ . The creation of an  $A_3$  singularity out of a smooth part of  $\mathcal{H}$  occurs generically via an  $A_4$  bifurcation, as is recalled in Figs. 1-3. Therefore it is natural within the MCT to imbed  $A_3$  scenarios in a discussion of the  $A_4$  singularity. The data reproduced above, show that this is indeed necessary for these polymers. Our analysis brings out that these systems do not show any relaxation features which cannot be interpreted qualitatively with an  $A_4$  scenario. MCT formulae for  $A_3$  or  $A_2$  cannot describe the qualitative features of e.g. PCTFE if the crystallinity becomes as large as 80%. Generically, a path  $\mathbf{V}(T)$  will not hit an  $A_3$  or an  $A_4$  singularity, since these points are located within the  $N$ -dimensional control parameter space  $\mathcal{H}$  on sets, which have only dimensionality  $N-2$  or  $N-3$  respectively. For nonvanishing  $\mathbf{V} - \mathbf{V}_c$  the solutions of (1.1)-(1.3) will differ from the leading order asymptotic formulae, discussed here and in the preceding work. In order to verify or disprove the applicability of the theory one has to vary two control parameters in case of  $A_3$  and three in case of  $A_4$  so that one approaches  $\mathbf{V}_c$  systematically. The range of frequencies, where the fit agrees with the data, should expand for  $\mathbf{V} - \mathbf{V}_c \rightarrow 0$ . It is hoped, that our results will lead to systematic extensions of the quoted experiments, so that such a test can be performed.

The formulae (2.10), (2.11), (2.16), (2.17) for the  $A_l$  scenario,  $l \geq 3$ , are so simple that one can offer them as phenomenological theory for the analysis of complex relaxation patterns. In case of  $A_3$ , the bifurcation scenario for the Weierstrass function is well known from applications of the differential Eq. (2.10) in classical mechanics. The fact that this approach still has some predictive power follows from the discussion in Sect. 4. But, let us reconsider the case for the most simple  $A_2$  scenario. Here the MCT explains the  $\beta$  minimum and suggests as interpolation for the spectrum  $\varepsilon''(\omega)/\varepsilon''_{\min} = [b \cdot (\omega/\omega_{\min})^a + a \cdot (\omega_{\min}/\omega)^b]/(a+b)$ . This is a 4-parameter fit formula using two fractals. Analogous fits

are in use for resonance peaks as Havriliak-Negami formulae. While the latter is a mere means of data interpolation the quoted expression for the  $\beta$  minimum has still predictive power. It implies relations between  $a$  and  $b$  and connections of the fractals with the temperature variation of the scales. These relations can be used in principle to verify or disprove the theory.

One of us (S.F.) gratefully acknowledges the support by the AvH-foundation and thanks M. Fuchs, A. Latz and V. Prigodin for helpful discussions.

## References

1. Arnold, V.I.: Catastrophe theory. 2nd. edn. Berlin, Heidelberg, New York: Springer 1986
2. Gilmore, R.: Catastrophe theory for scientists and engineers. New York: Wiley 1981
3. Götze, W.: In: Liquids, freezing and the glass transition. Hansen, J.P., Levesque, D., Zinn-Justin, J. (eds.), p. 287. Amsterdam: North Holland 1991
4. Forster, D.: Hydrodynamic fluctuations, broken symmetry and correlation functions. Benjamin Inc., Reading, 1975
5. Bengtzelius, U., Götze, W., Sjölander, A.: J. Phys. C17, 5915 (1984)
6. Götze, W., Sjögren, L.: J. Phys. C17, 5759 (1984)
7. Haussmann, R.: Z. Phys. B - Condensed Matter 79, 143 (1990)
8. Edwards, S.F., Anderson, P.W.: J. Phys. F5, 965 (1975)
9. Götze, W., Sjögren, L.: Z. Phys. B - Condensed Matter 65, 415 (1987)
10. Götze, W.: Z. Phys. B - Condensed Matter 60, 195 (1985)
11. Götze, W.: In: Amorphous and liquid materials. Lüscher, E. et al. (eds.), p. 34. Dordrecht: Martinus Nijhoff 1987
12. Sjögren, L.: In: Basic features of the glassy state. Alegria, A., Colmenero, J. (eds.), p. 137. Singapore: World Scientific 1990
13. Sjögren, L.: J. Phys.: Condensed Matter 3, 5023 (1991)
14. Götze, W., Sjögren, L.: Phys. Rev. A43, 5442 (1991)
15. Fuchs, M., Götze, W., Hildebrand, S., Latz, A.: Z. Phys. B - Condensed Matter 87, 43 (1992)
16. Li, G., Du, W.M., Chen, X.K., Cummins, H.Z., Tao, N.J.: Phys. Rev. A (in press 1991)
17. Götze, W., Sjögren, L.: J. Phys.: Condensed Matter 1, 4203 (1989)
18. Feller, W.: An introduction to probability theory and its applications. Vol. II, 2nd. edn., New York: Wiley 1966
19. Fuchs, M., Götze, W., Hofacker, I., Latz, A.: J. Phys.: Condensed Matter 3, 5047 (1991)
20. Scott, A.H., Scheiber, D.J., Curtis, A.J., Lauritzen, J.I., Hoffman, J.D.: J. Res. Natl. Bur. Stand. A66, 269 (1962)
21. Baker, W.O., Yager, W.A.: J. Am. Chem. Soc. 64, 2171 (1942)
22. Boyd, R.H.: J. Chem. Phys. 30, 1276 (1959)
23. McCall, D.M., Anderson, E.W.: J. Chem. Phys. 32, 237 (1960)
24. Curtis, A.J.: J. Res. Natl. Bur. Stand. A65, 185 (1961)
25. Pellegrini, B., Saletti, R., Terreni, P., Prudenziati, M.: Phys. Rev. B27, 1233 (1983)
26. Montroll, E.W., Shlesinger, M.F.: Proc. Natl. Acad. Sci. USA 79, 3380 (1982)
27. Montroll, E.W., Shlesinger, M.F.: In: Nonequilibrium phenomena II. From stochastics to hydrodynamics. Lebowitz, J.L., Montroll, E.W. (eds.). Amsterdam: Elsevier 1984
28. Montroll, E.W., Bendler, J.T.: J. Stat. Phys. 34, 129 (1984)
29. Weissman, M.B.: Rev. Mod. Phys. 60, 537 (1988)
30. Ishida, Y., Matsuo, M., Ito, H., Yoshino, M., Irie, F., Takayanagi, M.: Kolloid Z.Z. Polym. 171, 162 (1961)
31. Ishida, Y., Yamafuji, K., Ito, H., Takayanagi, M.: Kolloid Z.Z. Polym. 184, 97 (1962)
32. Schweizer, K.S.: J. Chem. Phys. 91, 5802; 5822 (1989)
33. Rostiasvili, V.G.: Sov. Phys. JETP 70, 563 (1990)